Institute of Physics Publishing — Classical and Quantum Gravity

Class. Quantum Grav. **22** (2005) S975–S984 doi:10.1088/0264-9381/22/18/S11

Calibration of TAMA300 in time domain

Souichi Telada[1], Daisuke Tatsumi[2], Tomomi Akutsu[3], Masaki Ando[4], Nobuyuki Kanda[5] and the TAMA Collaboration

[1] Length Standards Section, Advanced Industrial Science and Technology, Tsukuba, Ibaraki 305-8563, Japan
[2] National Astronomical Observatory of Japan, Mitaka, Tokyo 181-8588, Japan
[3] Institute for Cosmic Ray Research, University of Tokyo, Kashiwa, Chiba 277-8582, Japan
[4] Department of Physics, University of Tokyo, Hongo, Bunkyo-ku, Tokyo 113-0033, Japan
[5] Department of Physics, Graduate School of Science, Osaka City University, Sumiyoshi-ku, Osaka 558-8585, Japan

E-mail: souichi.telada@aist.go.jp

Received 11 April 2005, in final form 15 July 2005
Published 23 August 2005
Online at stacks.iop.org/CQG/22/S975

Abstract

We could reconstruct the strain of gravitational wave signals from acquired data in the time domain by using the infinite impulse response filter technique in TAMA300. We would like to analyse the waveform in the time domain for burst-like signal, merger phase waveform of binary neutron stars, and so on. We established the way to make a continuous time-series gravitational wave strain signal. We compared the time-domain reconstruction with the Fourier-space reconstruction. Both coincided within 3% in the observation range. We could also produce the voltage signal which would be recorded by the data-acquisition system from a simulated gravitational wave. This is useful for some analyses of simulations and signal injections. We could extract the waveform of the hardware injection signal in an observational run in the time domain. The extracted waveform was similar to the injection signal.

PACS number: 04.80.Nn

(Some figures in this article are in colour only in the electronic version)

1. Introduction

We have carried out nine observation runs in TAMA300. In the eighth observation run (DT8), over 1100 h of data were taken and the duty cycle was 81%. Also, hardware signal injection was achieved. Some simulated signals of gravitational waves were injected into the interferometer. In the ninth observation run (DT9), 556 h of data were taken and the best sensitivity of TAMA300 was recorded.

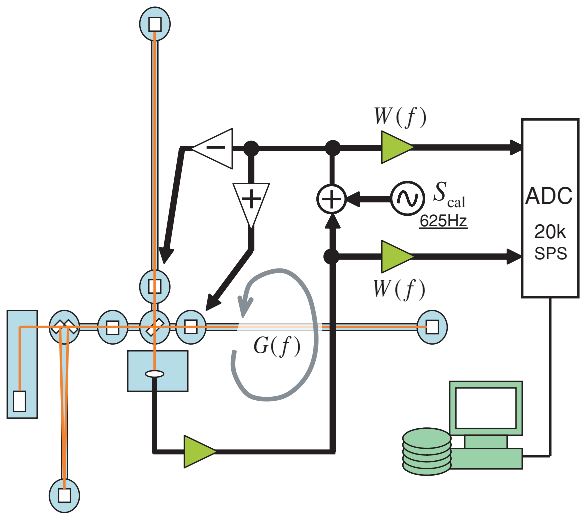

Figure 1. Optical configuration and L_- servo control of TAMA300. $G(f)$ is an open-loop transfer function of L_- servo. The feedback signal is acquired via a whitening filter, $W(f)$, by a computer. The signal is converted by an analog-to-digital converter whose sampling rate is 20 kSPS.

Although most data analyses for gravitational wave detectors have been analysed in Fourier space in TAMA300 [1], time-domain analyses are also important. Because acquired data are not exactly the same waveforms of gravitational wave signals, the data need to be reconstructed. It is easy to reconstruct them in Fourier space. GEO600 have reconstructed their data in the time domain [2, 3]. There is a difference between GEO600 and TAMA300 concerning the way to acquire data. It is thus difficult to reconstruct data in the time domain.

In a laser interferometer gravitational wave detector, many feedback servo controls are needed to keep the interferometer operating. In TAMA300, the most important is called the L_- feedback servo control, which is a differential length control of both 300 m Fabry–Perot arms of the interferometer, and whose signal is sensitive to gravitational wave signals. The unity gain of the L_- servo control was around 1 kHz, though the observation band was from 100 Hz to 2 kHz. For this reason, the interferometer signal was derived from the feedback signal to the test mass displacement of the interferometer. The signal was acquired through a whitening filter and an anti-aliasing filter by a computer with an analogue-to-digital converter. The acquired signals were distorted by the servo control, the actuator response, the whitening filter and the anti-aliasing filter. This 'distortion' should be corrected in order to obtain the strain of the gravitational wave signal. In Fourier-space analysis, we can easily correct 'distortion' by using transfer functions. For example, in the analysis of an inspiraling binary search with the matched filtering technique, we reconstructed the strain of a gravitational wave, $\tilde{h}(f)$, from the acquired voltage data, $\tilde{V}(f)$, by using the transfer function. We analysed the observation data for gravitational wave searches in Fourier space. It is necessary for various analyses to reconstruct them in the time domain. In the present work, we used the infinite impulse response filters technique to reconstruct in the time domain.

2. Optical configuration and servo control for TAMA300

Figure 1 shows the optical configuration and the L_- servo control of TAMA300. The light source is an injection-locked Nd:YAG laser whose wavelength is 1.064 μm, and the output power is 10 W. The laser beam travels through a triangle optical mode cleaner whose cavity length is about 10 m, and is then input into the main interferometer. The optical configuration of the main interferometer is a power-recycled Fabry–Perot Michelson interferometer. Both arm Fabry–Perot cavities are 300 m in length and their finesse is 500. As a result, they have a cavity pole of 500 Hz. The power-recycling gain is about 4.5. In the L_- servo control, an optical output signal is detected and changed to an electric signal by a photo detector made from a multi photo diode for a high power. The electric signal goes through electric servo filters, and is then fed back to the input of a coil–magnet actuator driver for displacements of mirrors that consist of Fabry–Perot cavities. The lengths of both Fabry–Perot cavities are controlled anti-symmetrically. The mirrors are suspended by double pendulums. For each mirror, four pairs of magnets on the mirror and coils on a cage of the pendulum consist of the actuator.

3. Data acquisition and calibration

The feedback signal to the coil–magnet actuator driver was derived and acquired by a computer with an analogue-to-digital converter. For real time calibration, we took the 'single peak calibration' method [4]. In order to obtain a change of the open-loop gain of the L_- servo control, a calibration signal was injected just before the coil–magnet actuator driver with a sum amplifier. The calibration signal was a sinusoidal wave of 625 Hz, which was generated by dividing the sampling frequency of 20 kHz of the analogue-to-digital converter by 32. The signals before and after the sum amplifier were acquired through whitening filters. We extracted 625 Hz components from the acquired signals before and after the sum amplifier, and then divided the before 625 Hz component by the after one. In this way, we could obtain an open-loop gain of 625 Hz. We thought that there were two changeable parameters in the L_- feedback servo. One was a dc gain and the other was the cavity pole of the Fabry–Perot cavity. We can know the change in the dc gain from the amplitude of the open-loop gain of 625 Hz, and can know the change in the cavity pole from the phase of the open-loop gain of 625 Hz. The dc gain is easily changed by changing the laser power, the alignment of the interferometer and so on. In fact, the dc gain was changed by about 10% during long-term operation. We had feared that the cavity pole would be changed by a deterioration of the mirror reflectance with contaminations. However, the cavity pole did not change during the observation runs. The amplitude and the phase of the open-loop gain in a part of DT8 are shown in figure 2.

4. Reconstruction of data in Fourier space

The acquired data by a computer are time-series data in the dimension of voltage. We need to reconstruct the strain of the gravitational wave. In this section, we describe how to produce it in Fourier space. We transform to a Fourier spectrum of the voltage data from the time-series voltage data with FFT. A mirror displacement of the L_- servo appears at the feedback signal just before the coil–magnet actuator driver according to the following equation:

$$\tilde{x}(f) = A(f)\frac{1+G(f)}{G(f)}\tilde{V}_{\mathrm{feedback}}(f), \tag{1}$$

where $\tilde{x}(f)$ and $\tilde{V}_{\mathrm{feedback}}(f)$ are the Fourier spectrum of the mirror differential displacement and the feedback signal, respectively. $G(f)$ is an open-loop transfer function of the L_- servo control. $A(f)$ is a transfer function from the input-voltage signal of the coil–magnet actuator driver to the mirror displacement. This transfer function is basically formed by a second-order low-pass filter, whose cutoff frequency is the same as the resonant frequency of the pendulum.

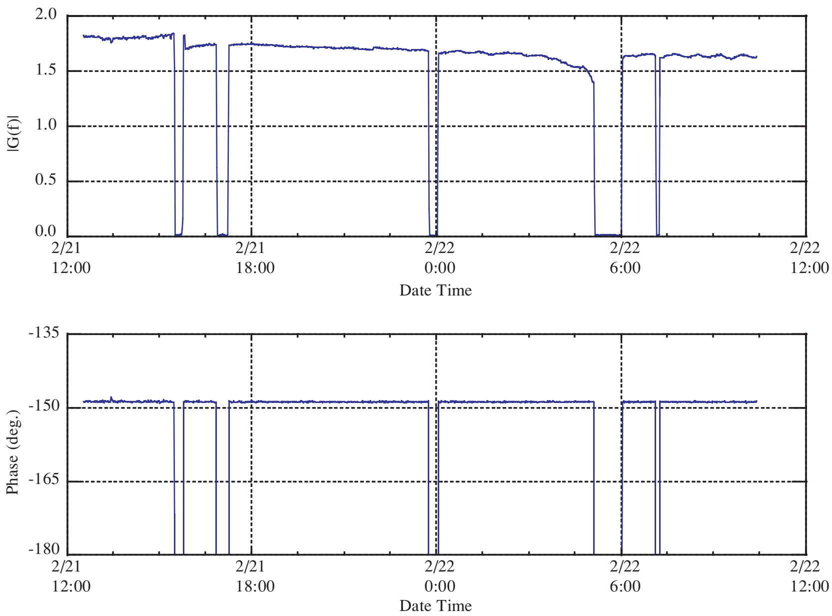

Figure 2. Fluctuation of the open-loop transfer functions in DT8 which ran from 14 February 2003 to 15 April 2003. The upper graph is the absolute value of the gain and the lower graph is the phase. The interferometer was unlocked when the absolute value of the gain was zero.

If $|G(f)| \gg 1$, $\frac{1+G(f)}{G(f)}$ is almost unity and insensitive to a change of the open-loop transfer function. On the other hand, in a frequency region above the unity gain frequency, $\frac{1+G(f)}{G(f)}$ is sensitive to that, and at close to the unity gain frequency, it is more sensitive. Since the unity gain frequency of TAMA300 is in the observation range, the open-loop transfer function and its fluctuation are particularly important.

The feedback signal is derived and goes through a whitening filter. The whitening filter cuts off higher and lower frequency components of the feedback signal for a dynamic range of the analogue-to-digital converter. The relationship between the acquired data and the feedback signal is shown by the following equation:

$$\tilde{V}_{\mathrm{ADC}}(f) = W(f)\tilde{V}_{\mathrm{feedback}}(f), \tag{2}$$

where $\tilde{V}_{\mathrm{ADC}}(f)$ is the Fourier spectrum of the acquired data and $W(f)$ is the transfer function of the whitening filter.

Since the base-line length is 300 m, we obtain the strain of the gravitational wave by dividing $\tilde{x}(f)$ by 300 m. We can thus reconstruct from the acquired data the strain of the gravitational wave using the following equation:

$$\tilde{h}(f) = \frac{1}{300\mathrm{m}} \frac{1}{W(f)} A(f) \frac{1+G(f)}{G(f)} \tilde{V}_{\mathrm{ADC}}(f), \tag{3}$$

where $\tilde{h}(f)$ is the Fourier spectrum of the strain of a gravitational wave.

5. Reconstruction of data in the time domain

We used an infinite impulse response (IIR) filter to reconstruct in the time domain. In another method, the combination of FFT and inverse FFT is used. In this method, the Fourier spectrum of $\tilde{h}(f)$, which is reconstructed as explained in the previous section, is transformed into $h(t)$ by the inverse FFT. Although this is a conventional way, there are some problems. On a gravitational wave detector, continuous observation is necessary. We acquire very large data, and have to analyse such data in order to search for gravitational wave signals. It is impossible that such large data are transformed by using FFT in one block. Thus, in the case of the FFT and inverse-FFT combination method, it is necessary to divide the data. By dividing the data, there is large effect on the data especially close to the edge. In addition, the time window for FFT and inverse FFT affects the gravitational wave signal as the distortion. If the signal is placed on the edge of the continuous block, the waveform will be distorted due to the window effect, or divided into two blocks. As we would like to obtain continuous time-series data, we thus adopted an impulse response filter in a digital-filter technique.

5.1. *Infinite impulse response (IIR) filter*

There are two types of impulse response filters. One is the finite impulse response (FIR) filter, and the other is the infinite impulse response (IIR) filter. When the input time-series discrete data to the filter is I_n and the output one from the filter is O_n, where n is the time index, the impulse response filter is defined as

$$O_n = \sum_{k=0}^{M} c_k I_{n-k} + \sum_{j=1}^{N} d_j O_{n-j}, \tag{4}$$

where c_k and d_j are coefficients and define the filter response. If $N = 0$, so that there is no second term in equation (4), then it is FIR, else IIR. Since IIR is superior to FIR with same number of coefficients, we used IIR for reconstruction. The servo filter and the whitening filter were constructed from analogue filters. We thus need IIR filters with the same response as the analogue filters. For example, in the case of a first-order low-pass filter with a cutoff frequency of f_c, the coefficients set of the IIR filter is

$$c_0 = \frac{1}{1 + \frac{2}{2\pi f_c \Delta t}}, \qquad c_1 = \frac{1}{1 + \frac{2}{2\pi f_c \Delta t}}, \qquad d_1 = \frac{1 - \frac{2}{2\pi f_c \Delta t}}{1 + \frac{2}{2\pi f_c \Delta t}}, \tag{5}$$

$$M = 1, \qquad N = 1, \tag{6}$$

where Δt is the sampling interval of the analogue-to-digital converter. IIR filters can emulate analogue filters well, but not completely. There are differences between an IIR filter and an analogue filter, especially in the higher frequency region, or in other words, near the sampling frequency. We made special IIR filter coefficients sets, $\{c_k, d_j\}$, which have smaller differences than the general coefficient sets in the observation range [5]. For example, although the general coefficient set of a first-order low-pass filter is as equations (5) and (6), our coefficient set of that is

$$c_0 = \frac{1}{1 + \frac{147}{60}\frac{1}{2\pi f_c \Delta t}}, \tag{7}$$

$$d_1 = \frac{6\frac{1}{2\pi f_c \Delta t}}{1 + \frac{147}{60}\frac{1}{2\pi f_c \Delta t}}, \qquad d_2 = -\frac{\frac{15}{2}\frac{1}{2\pi f_c \Delta t}}{1 + \frac{147}{60}\frac{1}{2\pi f_c \Delta t}}, \qquad d_3 = \frac{\frac{20}{3}\frac{1}{2\pi f_c \Delta t}}{1 + \frac{147}{60}\frac{1}{2\pi f_c \Delta t}}, \tag{8}$$

$$d_4 = -\frac{\frac{15}{4}\frac{1}{2\pi f_c \Delta t}}{1 + \frac{147}{60}\frac{1}{2\pi f_c \Delta t}}, \qquad d_5 = \frac{\frac{6}{5}\frac{1}{2\pi f_c \Delta t}}{1 + \frac{147}{60}\frac{1}{2\pi f_c \Delta t}}, \qquad d_6 = -\frac{\frac{1}{6}\frac{1}{2\pi f_c \Delta t}}{1 + \frac{147}{60}\frac{1}{2\pi f_c \Delta t}}, \tag{9}$$

$$M = 0, \qquad N = 6. \tag{10}$$

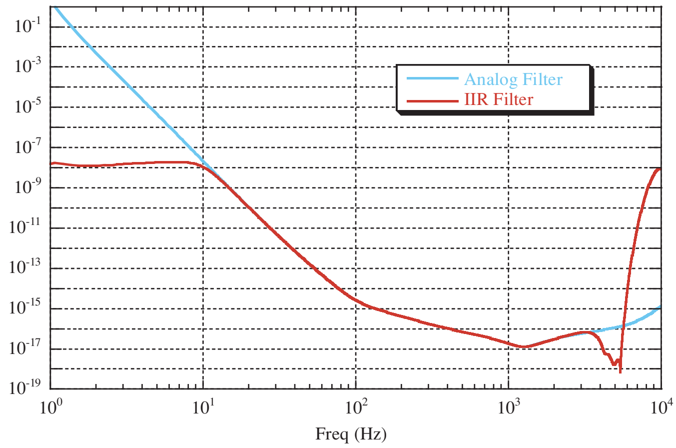

Figure 3. Transfer functions of the IIR filter and the analogue filter. The blue (grey) line is the total transfer function to convert from the acquired voltage signal to the strain of a gravitational wave in Fourier space. The red (black) line is the frequency response of the IIR filter. The difference below 10 Hz is caused by the additional high-pass filter for the IIR.

In this way, our coefficient sets have more coefficients than the general coefficient sets do. In addition, we produced a special function to calculate a closed-loop transfer function [5].

5.2. Difference between the frequency model and the time-domain model

In order to clear up the difference between reconstruction in the time domain and reconstruction in Fourier space, we compared those transfer functions. We could calculate the transfer function of our IIR filter to reconstruct from the time-series acquired voltage signal, $V_{\mathrm{ADC}}(t)$, to the time-series strain of a gravitational wave, $h(t)$. It is shown in figure 3 along with the analogue filter transfer function. In the higher frequency region, there are differences because even our IIR filter emulates the analogue filter incompletely. In the lower frequency region, differences are caused by an additional high-pass filter. In the whitening filter, lower frequency components are cut off with the high-pass filter. As the inverse-whitening filter is operated, the lower frequency components and dc component became extremely big and infinite. For this reason, the inverse whitening filter cannot be calculated by a computer. Therefore, we used the additional filter in the inverse-whitening filter to fold down below 10 Hz. The amplitude ratio and the phase difference between the frequency model and the time-domain model are shown in figure 4. The error of the amplitude ratio was within 3% in the observation range from 100 Hz to 2 kHz. If there is no additional filter in the inverse-whitening filter, the amplitude ratio is almost unity, and the phase difference is almost zero degree in the lower frequency region.

5.3. Reconstructed data in Fourier space and the time domain

In order to compare the time-domain reconstruction with the Fourier-space reconstruction, the time-domain reconstructed data were transformed to the Fourier spectrum. In the Fourier-space reconstruction, $V_{\mathrm{ADC}}(t)$ was transformed to $\tilde{V}_{\mathrm{ADC}}(f)$ with FFT, and was then reconstructed to $\tilde{h}(f)$. In the time-domain reconstruction, $V_{\mathrm{ADC}}(t)$ was reconstructed to $h(t)$, and then transformed to $\tilde{h}(f)$ with FFT. Figure 5 shows the reconstructed sensitivities in DT9. They

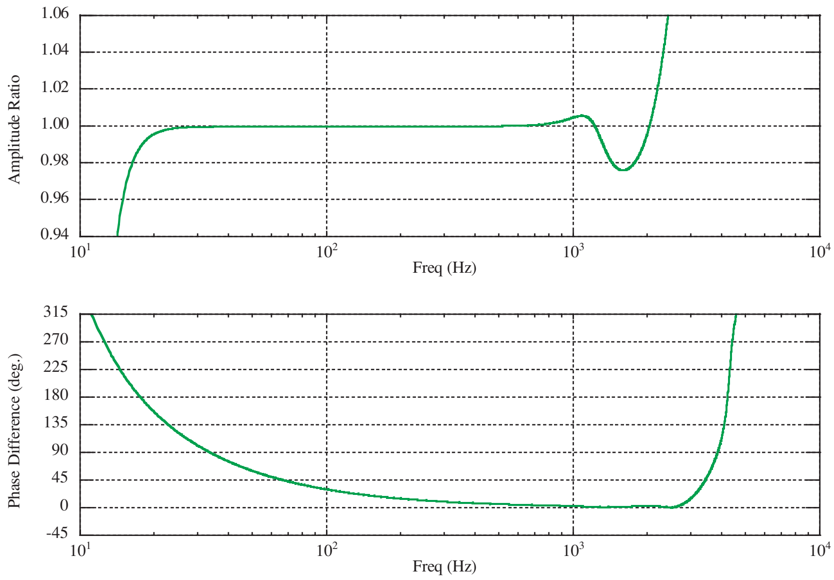

Figure 4. Difference between the IIR and the analogue filter. The upper graph is the amplitude ratio and the lower graph is the phase difference. There is a small effect of the additional high-pass filter for the amplitude ratio, but a large effect for the phase difference.

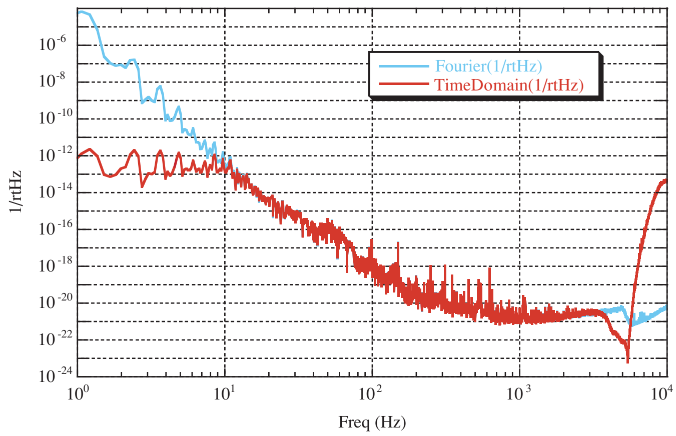

Figure 5. Sensitivity of TAMA300 in DT9. The blue (grey) line is the Fourier-space reconstruction and the red (black) line is the time-domain reconstruction.

show good agreement in the observation range. Just before the analogue-to-digital converter, there was an anti-aliasing filter, whose cutoff frequency is 5 kHz. Since the sensitivity was limited by the resolution of the analogue-to-digital converter over 5 kHz, which was out of observation range, we ignored the anti-aliasing filter for the reconstructions.

5.4. Time-domain signals

We can also produce a voltage signal, $V_{\mathrm{ADC}}(t)$, from a simulated gravitational wave, $h(t)$, with the IIR. It is useful for software signal injection and some analyses in the time domain.

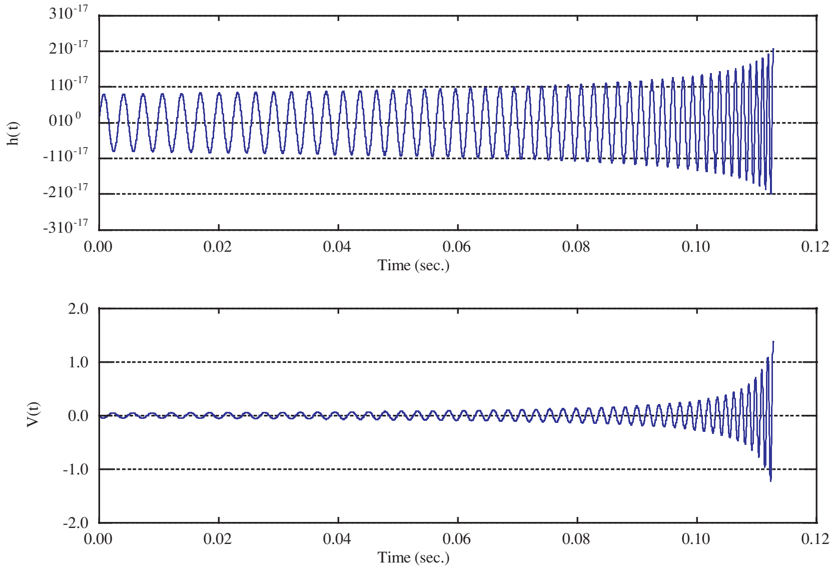

Figure 6. Chirp signal of $h(t)$ and $V_{\mathrm{ADC}}(t)$. The upper graph shows the simulated chirp signal, which comes from a 1.4–1.4 solar-mass inspiraling binary neutron star. The lower graph shows the waveform that appears in the acquired data when the chirp signal comes.

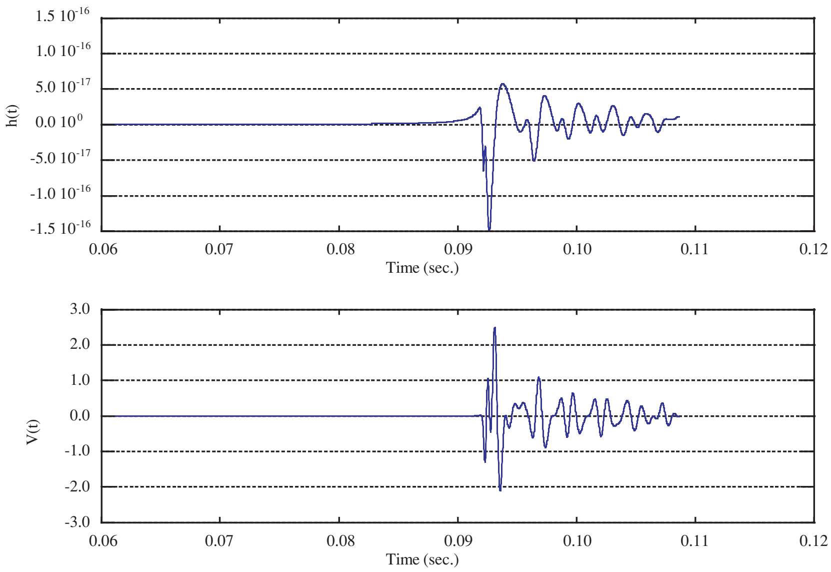

Figure 7. Burst signal of $h(t)$ and $V_{\mathrm{ADC}}(t)$. The upper graph shows the burst signal of A1B1G1_N of Dimmelmeier's burst catalogue. The lower graph shows the voltage signal of $V_{\mathrm{ADC}}(t)$.

Figures 6 and 7 show a chirp signal and a burst signal, respectively. The chirp signal is expected from inspiraling binary neutron stars whose masses are 1.4 solar mass. The amplitude in $V_{\mathrm{ADC}}(t)$ grows bigger than that in $h(t)$ near the merger phase. The burst signal

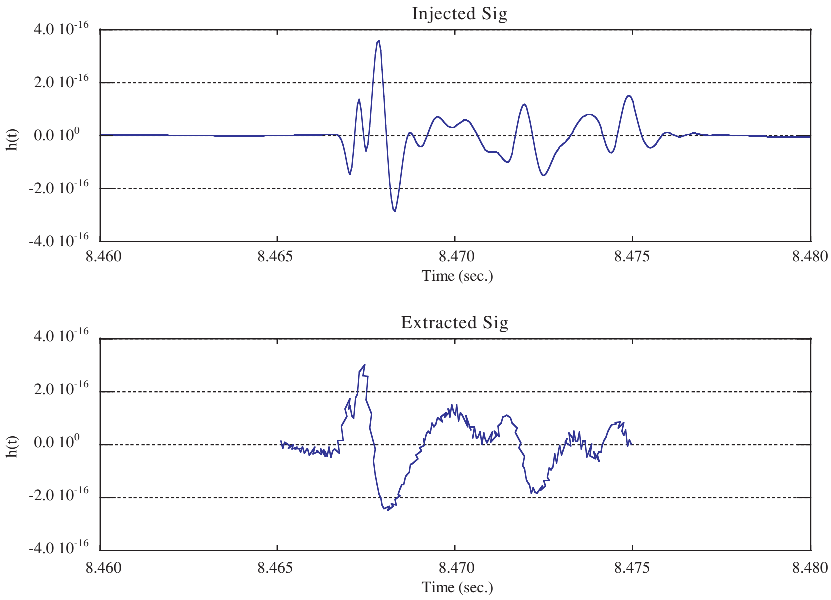

Figure 8. Injection signal and extracted waveform. The upper graph shows the hardware injection signal and the lower graph shows the extracted waveform. Similar signals appear at the same time.

is from Dimmelmeier's burst catalogue (no A1B1G1_N) [6, 7]. Because burst signals have complex waveforms, $V_{\mathrm{ADC}}(t)$ and $h(t)$ are not very similar.

5.5. Extraction of hardware injection signals

In DT8, some simulated gravitational wave signals were injected into the interferometer. This is called hardware signal injection. We extracted the injected signal in the reconstructed data and compared the extracted waveform with the injected signal. Because the reconstructed data had large noises of higher and lower frequencies, we operated on the reconstruct data for a band-pass filter of the IIR filter. We could extract a similar waveform to the injection signal. The injection signal and the extracted waveform are shown in figure 8. This is one burst signal of the injection signals.

6. Discussion and concluding remarks

We could reconstruct the data in the time domain whose error was within 3% in the observation range. For the additional filter, there are differences between the time-domain reconstruction and the Fourier reconstruction. In this work, the additional filter was also made from an IIR filter. One can make some FIR filters which cut off high and/or low frequency components without changing the phase. If such a FIR filter is used as the additional filter, there is no phase difference. However, FIR filters take more time to calculate. Thus, it does not suit the analysis of a gravitational wave search. In a gravitational wave search with a time-domain matched filtering technique, the effect of this large phase difference is reduced by operating with the same IIR additional filter on the template waveform. We can cancel the phase distortion in gravitational wave search analysis. However, when we catch a gravitational wave, the detected waveform is very important for gravitational wave astronomy. We thus think that a

FIR additional filter, which is no phase distortion, is an essential technique even if it takes more time to calculate.

We demonstrated how to extract the waveform of a hardware injection signal in reconstructed data. The waveform is similar to the waveform of the injection signal, but not completely. We think that this is caused by using a conventional way to reduce noises. The acquired data have some large noises, such as the calibration signal, power-line noise and its harmonics. These are well known and can be removed in the time domain. If the noises are reduced, the extracted waveform will be more precise to the injection signal. We plan to conduct some analyses in the time domain.

References

[1] Tagoshi H *et al* 2001 *Phys. Rev.* D **63** 062001
[2] Hewitson M *et al* 2003 *Class. Quantum Grav.* **20** S885
[3] Hewitson M *et al* 2003 *Rev. Sci. Instrum.* **74** 4184
[4] Telada S *et al* 2000 *Gravitational Wave Detection II (Proc. 2nd TAMA Workshop)* p 129
[5] Telada S *et al* to be published
[6] Dimmelmeier H *et al* 2002 *Astron. Astrophys.* **388** 917
[7] Dimmelmeier H *et al* 2002 *Astron. Astrophys.* **393** 523